optica

Stable subpicosecond soliton fiber laser passively mode-locked by gigahertz acoustic resonance in photonic crystal fiber core

M. Pang,[1,*] X. Jiang,[1] W. He,[1] G. K. L. Wong,[1] G. Onishchukov,[1] N. Y. Joly,[1] G. Ahmed,[1] C. R. Menyuk,[2] and P. St.J. Russell[1]

[1]Max Planck Institute for the Science of Light, Guenther-Scharowsky-Strasse 1, 91058 Erlangen, Germany
[2]Department of Computer Science and Electrical Engineering, University of Maryland Baltimore County, Baltimore, Maryland 21250, USA
*Corresponding author: meng.pang@mpl.mpg.de

Received 17 November 2014; revised 9 March 2015; accepted 10 March 2015 (Doc. ID 227058); published 30 March 2015

Ultrafast lasers with high repetition rates are of considerable interest in applications such as optical fiber telecommunications, frequency metrology, high-speed optical sampling, and arbitrary waveform generation. For fiber lasers mode-locked at the cavity round-trip frequency, the pulse repetition rate is limited to tens or hundreds of megahertz by the meter-order cavity lengths. Here we report a soliton fiber laser passively mode-locked at a high harmonic (~2 GHz) of its fundamental frequency by means of optoacoustic interactions in the small solid glass core of a short length (60 cm) of photonic crystal fiber. Due to tight confinement of both light and vibrations, the optomechanical interaction is strongly enhanced. The long-lived acoustic vibration provides strong modulation of the refractive index in the photonic crystal fiber core, fixing the soliton spacing in the laser cavity and allowing stable mode-locking, with low pulse timing jitter, at gigahertz repetition rates.

OCIS codes: (140.4050) Mode-locked lasers; (060.5295) Photonic crystal fibers; (060.5530) Pulse propagation and temporal solitons.

http://dx.doi.org/10.1364/OPTICA.2.000339

Optical fibers provide an excellent platform for ultrafast lasers, offering many advantages compared to bulky, free-space counterparts, including high beam quality, efficient heat dissipation, and compact and simple configurations with no need for alignment [1–4]. A limitation of ultrafast fiber lasers, however, is that it is difficult to generate pulses at gigahertz repetition rates [1,4]. Typical fiber lasers [5–7] have round-trip frequencies of tens or hundreds of megahertz, limited by the long cavity lengths [4]. To increase the round-trip frequency up to several gigahertz, ultrashort (centimeter-scale) cavity lengths are necessary [8–11]. In order to increase the pulse repetition rate of conventional fiber lasers, several active [12–14] and passive [15–19] harmonic mode-locking schemes have been proposed, allowing equally spaced multipulses to circulate in the laser cavity. In active schemes with either amplitude or phase modulation, expensive radio-frequency (RF) sources and modulators are used, which increases the laser complexity [4]. For passive schemes, one solution is to incorporate subcavities to fix the pulse repetition rate at a harmonic of the fundamental cavity frequency [15,16], but this requires sophisticated stabilization electronics to balance the optical phase instabilities between the major and subsidiary cavities. Another possible passive scheme makes use of temporally long-range interactions between pulses [17–20]. Such long-range pulse interactions are, however, very week in the conventional single-mode fiber (SMF) [5,17–20], resulting in erratic repetition rates and large pulse timing jitter.

Recently, enhancement of optomechanical interactions by tight field confinement has been reported in photonic crystal fibers (PCFs) [21–23]. In a silica–glass solid-core PCF with high air-filling fraction, simultaneous confinement of light and mechanical vibrations within a small core area leads to high optical and acoustic energy intensities and a large optoacoustic overlap, resulting in an enhancement of the optoacoustic effect by around two orders of magnitude [21,22]. Moreover, PCFs with core diameters of ~1 μm support gigahertz acoustic resonances, and can be easily integrated into conventional fiber lasers [24].

In this Letter, we report that the pulse repetition rate of a soliton fiber laser can be passively locked to a gigahertz acoustic resonance in the solid core of a 60-cm-long silica PCF, corresponding to a very high-order harmonic N of the cavity round-trip frequency f_{RT} (a few megahertz). We achieve hyperbolic secant pulses with subpicosecond durations—much shorter than in previous work [25–27]. The tunability of the repetition rate, pulse amplitude noise, and timing jitter are also explored.

The fiber laser configuration and diagnostic setup are shown in Fig. 1. In the unidirectional ring cavity, a 0.6 m length of Er-doped fiber (EDF) with peak absorption of 110 dB/m at 1530 nm is used as the gain medium, and two 976 nm laser diodes (LDs) provide continuous-wave pump light. Two polarization controllers (PC 2 and PC 3), a polarizer, and a 0.2 m length of highly nonlinear fiber were necessary to realize a fast saturable absorber [28,29]. A tunable delay line was used to alter the cavity length, and a 90:10 fiber coupler provided the laser output.

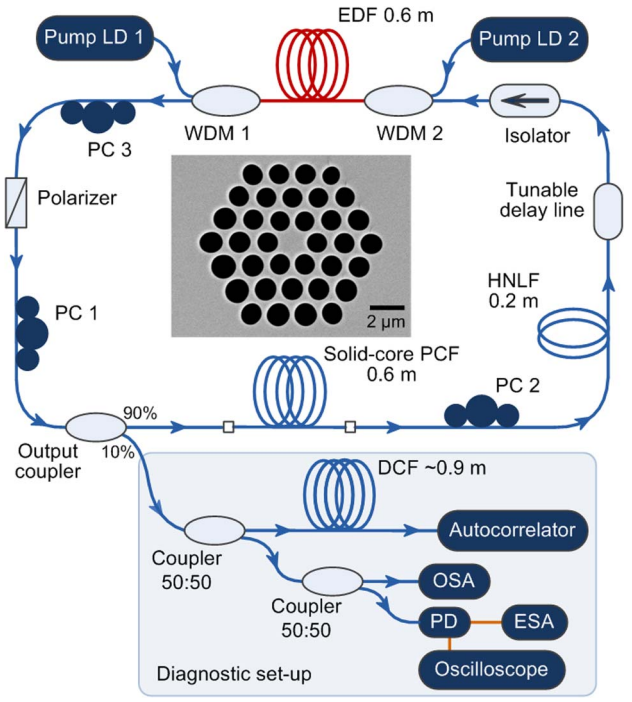

Fig. 1. Experimental setup and SEM of the solid-core PCF. EDF, Er-doped fiber; LD, laser diode; WDM, wavelength division multiplexer; PC, polarization controller; HNLF, highly nonlinear fiber; DCF, dispersion compensating fiber; OSA, optical spectrum analyzer; PD, photodetector; ESA, electrical spectrum analyzer.

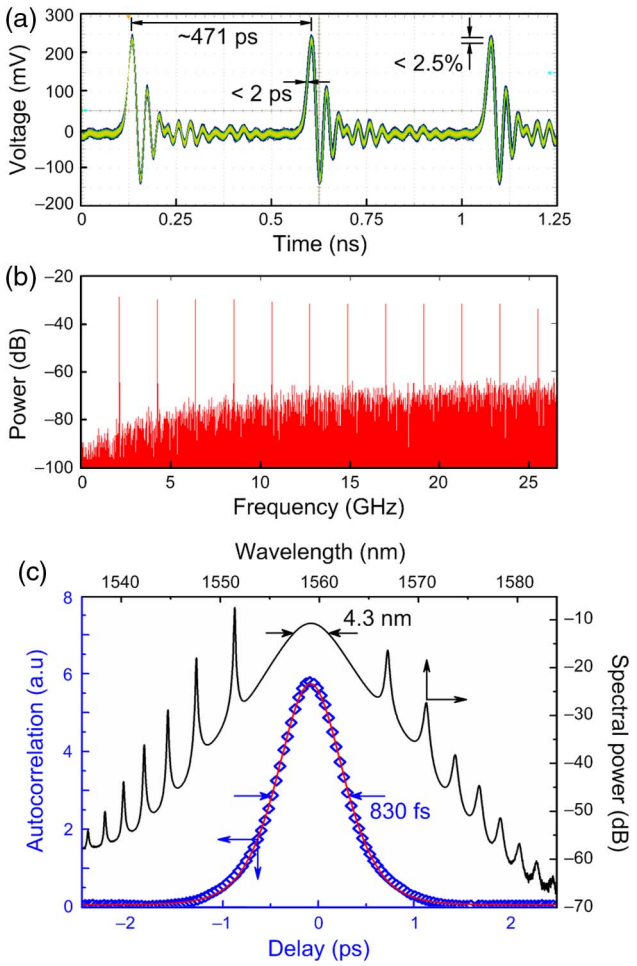

Fig. 2. Experimental results. (a) typical pulse train recorded over 30 min using an oscilloscope operating in the infinite persistence mode. (b) RF spectrum of the pulse train measured by the ESA. (c) left-hand axis: measured autocorrelation of the output pulses (blue circles), plotted against the delay time of the autocorrelator (bottom axis), and the hyperbolic secant fit (red solid line) of the measured data. Right-hand axis: measured optical spectrum of the laser, plotted against wavelength (top axis). Kelly sidebands are clearly visible.

A 0.6 m length of solid-core silica PCF [see the scanning electron micrograph (SEM) in Fig. 1] was used. The core diameter (d_{core}) was ~1.8 μm, and the air-filling fraction (r_{air}) ~0.53. A polarization controller (PC 1) was used in front of the PCF so as to ensure that linearly polarized light was launched into one of the principal polarization axes of the fiber. The measured birefringence was $\sim 1.5 \times 10^{-4}$ at 1560 nm, which corresponds to a beat-length of ~10 mm and ensures efficient suppression of polarization mode coupling. All the other components in the laser cavity were made from conventional SMF. In order to reduce the splicing loss between PCF and SMF, a ~1 cm length of ultrahigh-numerical-aperture fiber was used to form a transition [24]. The total SMF–PCF–SMF loss was ~3 dB, including the intrinsic PCF loss (<0.05 dB/m measured by the cut-back method). The total cavity loss was ~6 dB, and the cavity mode spacing was 16.8 MHz, corresponding to a total cavity length of 12.2 m.

In the diagnostic setup, an autocorrelator was used to measure the pulse duration. In front of the autocorrelator, a section of ~0.9 m dispersion compensating fiber (DCF), with normal dispersion of 55 ps^2/km at 1560 nm, was used to compensate the anomalous dispersion of the ~2 m length of conventional SMF patch cord. The pulse spectrum was measured using an optical spectrum analyzer with a 0.01 nm resolution, and the time-domain pulse train and its RF spectrum were recorded using a 33 GHz photodetector, a 33 GHz oscilloscope, and a 26.5 GHz electrical spectrum analyzer (ESA).

Lasing commenced at ~60 mW, noisy pulsations appearing just above this pump power. When the pump power was increased further to ~550 mW, and all three PCs and the tunable delay line were carefully adjusted, a clear transition from a noisy signal to a stable high-harmonic mode-locked pulse train was observed. At these higher pump powers, the laser always started up in high-harmonic mode. After turning off and restarting the laser, only fine-tuning of the polarization controllers was required for the stable high-harmonic mode-locking to be recovered. At a pump power of 670 mW, the time-domain pulse train was recorded over 30 min using an oscilloscope working in infinite persistence mode; a typical measurement is shown in Fig. 2(a). A stable gigahertz pulse train was observed with a long-term amplitude instability of <2.5% root-mean-square (rms) and a pulse timing jitter <2 ps rms (the measurement was limited by the ~1.7 ps intrinsic timing jitter of the oscilloscope). The RF spectrum of the pulse train measured by an ESA is shown in Fig. 2(b). The peak at 2.1221 GHz and its integer multiples correspond to mode-locking at the 126th harmonic of the fundamental cavity frequency. All other cavity harmonics are suppressed with a side-mode suppression ratio greater than 50 dB.

The pulse autocorrelation function is shown in Fig. 2(c). The full width half-maximum (FWHM) pulse duration is ~540 fs,

estimated by fitting the data to a hyperbolic secant function (autocorrelation function width 830 fs). The optical spectrum of the laser output is also shown in Fig. 2(c). It has an optical bandwidth of ~4.3 nm, and the time-bandwidth product of ~0.3 is close to the transform limit for a hyperbolic secant pulse. Strong Kelly sidebands [30] in the optical pulse spectrum indicate that the fiber laser is operating in the soliton regime.

The laser shows good long-term stability. Monitoring the 2.1221 GHz peak using the ESA for 1 h revealed that it drifted slowly within a 5 kHz range, corresponding to a relative long-term fluctuation in repetition rate of less than 2.5 parts per million. We also ran the laser continuously over 10 h without observing any pulse degradation.

The short-term pulse amplitude noise and timing jitter were estimated by measuring the single-sideband (SSB) noise spectra for the baseband and different harmonics of the pulse repetition rate [31,32] (see Supplement 1). By integrating the baseband noise of the laser, we estimated the relative amplitude noise of the laser to be ~0.1% over a bandwidth of 1 Hz to 1 MHz [31]. The SSB phase noise spectra of the first, fourth, and eighth harmonics, measured in the frequency range from 100 Hz to 1 MHz, were used to estimate the short-term pulse timing jitter, giving a value of ~40 fs over a bandwidth of 100 Hz to 1 MHz [31] (see Supplement 1).

In the experiments we investigated the dependence of the pulse duration and optical bandwidth on the intracavity pulse energy. By varying the pump power level, the FWHM pulse duration and 3 dB optical bandwidth were measured for different intracavity pulse energies. The results are plotted in Fig. 3. When the pulse energy was increased from 21 to 38 pJ, the pulse duration decreased from 670 to 450 fs while the optical bandwidth increased from 3.6 to 4.9 nm. As also shown in Fig. 3, the time-bandwidth product remained almost constant at ~0.3, indicating that the laser was operating in the soliton regime. The deviation at high pulse energies between data and fitted curves (based on the fundamental soliton assumption [33]) is mainly due to increasing conversion to Kelly sidebands [30] as shown in Fig. 2(c).

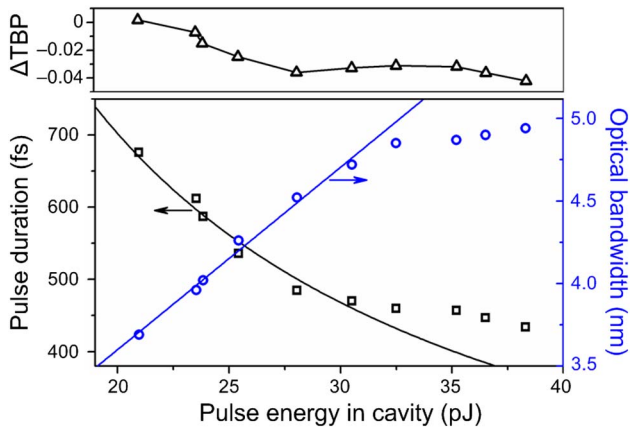

Fig. 3. Measured dependence of pulse parameters on intracavity pulse energy. Upper left-hand axis: deviation of pulse time-bandwidth product (ΔTBP) from 0.31 (black triangles), plotted against estimated pulse energy in laser cavity. Lower left-hand axis: measured FWHM pulse duration (black squares) fitted to Eq. (2) (full black line). Right-hand axis: measured 3 dB optical bandwidth of the pulses (blue circles) fitted to Eq. (2) using TBP = 0.31 (full blue line).

By changing the length of the delay line in the laser cavity (shown in Fig. 1), the repetition rate could be varied continuously over a range of ~9.6 MHz (from 2.1161 to 2.1257 GHz, corresponding to a cavity length tuning of ~80 mm), while the laser remained stably mode-locked. During this process the pulse duration remained almost constant at 540 fs (the deviation is within the ±30 fs measurement accuracy of the autocorrelator).

We measured the comb structure of the laser using a heterodyne method, employing a fiber laser with a 2 kHz linewidth as the local oscillator. The results (see Supplement 1) show a comb of frequencies spaced by the cavity round-trip frequency f_{RT}. The nth comb line is optoacoustically coupled to every $(n + mN)$th comb line, where Nf_{RT} is the harmonic mode-locking frequency and m the order of the mth high-harmonic comb line. Thus the spectrum consists of many interleaved but independent gigahertz combs, each of which alone would produce a coherent train of mode-locked soliton pulses. Because, however, each comb is spaced apart from the others by multiples of the cavity round-trip frequency, and the combs have random relative phases, the result is a train of uncorrelated soliton pulses. Although there is no particular phase relationship among the 126 solitons within the laser cavity, the acoustic resonance in the PCF core forces the temporal spacing between the pulses to remain constant.

The principle of passive mode-locking to an acoustic resonance in the core of a PCF can be simply explained as follows: in the steady state, the gigahertz pulse train, propagating in the solid-core PCF, drives a trapped acoustic wave through electrostriction. The index modulation produced by the vibration acts in turn on the driving pulses. The enhanced optoacoustic effect in the small area of the PCF core allows successive pulses to interact, efficiently stabilizing the pulse spacing in the fiber laser cavity and suppressing pulse timing jitter.

Optically driven acoustic vibrations, tightly guided in the PCF core, have been studied in detail by Kang *et al.* [22]. In practice, only the fundamental radial (R_{01}) acoustic mode is considered because this acoustic mode is most efficiently excited by the fundamental optical mode. In experiments the repetition frequency of the driving pulses ($\Omega/2\pi = Nf_{RT}$) is equal to an integer multiple N of the round-trip frequency f_{RT}, which is determined by the cavity length, while the resonant frequency of the R_{01} acoustic mode (Ω_{01}) is mainly determined by the PCF structure. We denote the offset between them as $\delta = \Omega - \Omega_{01}$. In the steady state a train of pulses with energy E_P and duration much shorter than the acoustic period can drive a modulation of the relative permittivity of the glass (in the form of an acoustic wave ρ; see Supplement 1) as

$$\Delta\varepsilon_r(z,t,r,\theta) = \gamma_e\frac{\rho}{\rho_0} = \frac{\gamma_e^2|Q|E_p\rho_{01}(r,\theta)e^{i(\Omega t - qz - \Delta\varphi)}}{4\pi n_{\text{eff}}cA_{\text{eff}}\rho_0\sqrt{4\delta^2+\Gamma_B^2}} + \text{c.c.}, \tag{1a}$$

$$\Delta\varphi = \operatorname{arccot}(-2\delta/\Gamma_B), \qquad 0 \le \Delta\varphi \le \pi, \tag{1b}$$

where γ_e and ρ_0 are the electrostrictive coefficient and density of silica, n_{eff} and A_{eff} are the effective refractive index and mode area of the fundamental optical mode in the PCF, c is the speed of light in vacuum, $\rho_{01}(r,\theta)$ is the dimensionless acoustic profile of the R_{01} acoustic mode, q is its propagation constant along the PCF axis, and Γ_B is its Brillouin linewidth. The overlap

integral Q between the fundamental optical mode and the R_{01} acoustic mode is defined in Supplement 1. As shown in Eq. (1a), the acoustic wave frequency equals the pulse repetition frequency, while the phase matching condition requires that the propagation constant of the acoustic wave equals that of the driving pulses [22,34]. Acoustic gain appears when the phase shift $\Delta\varphi$ between the driving pulse train and the acoustic wave [Eq. (1b); see Supplement 1] lies within the range $(0, \pi)$ [34].

The light-driven acoustic core resonance, operating as a phase modulation, acts back on the light, fixing the soliton spacing inside the laser cavity. The passive pulse-spacing stabilization can be understood most intuitively as an enhancement of temporally long-range pulse interactions by the coherent excitation of an acoustic vibration tightly confined in the PCF core, and is somewhat similar to active mode-locking by regenerative feedback [35,36], except that no high-frequency electronic components such as photodiodes, amplifiers, or band-pass filters are required.

The acoustic gain bandwidth of the PCF was measured to be ~8 MHz [22], corresponding to an acoustic quality factor of ~250 (see Supplement 1). For stable high-harmonic mode-locking, the tunable delay line must be adjusted so as to place one harmonic of the cavity mode spacing within the acoustic gain bandwidth. Continuous tuning of the pulse repetition rate can be achieved by adjusting the cavity length, but only if the cavity harmonic remains within the acoustic gain bandwidth, ensuring that the light-driven acoustic resonance in the PCF remains strong enough to lock the pulse positions.

Since the pulse duration (subpicosecond) is much shorter than the period of acoustic oscillation (~470 ps), it is much more strongly affected by Kerr-related self-phase modulation than by the optoacoustic effect. Note also that self-amplitude modulation in the saturable absorber is much weaker than self-phase modulation in the cavity (see Supplement 1). In a laser cavity with anomalous average dispersion, the pulse duration is thus dominated by the formation of sech^2 fundamental solitons [33] of energy E_P and FWHM pulse duration τ_{FWHM}:

$$E_P \tau_{\mathrm{FWHM}} = \frac{-3.52\beta_2}{\gamma_{\mathrm{Kerr}}}, \tag{2}$$

where β_2 is the average group-velocity dispersion and γ_{Kerr} is the average Kerr nonlinearity coefficient in the cavity (estimated to be $-21.9\ \mathrm{ps}^2/\mathrm{km}$ and $-3.4\ \mathrm{km}^{-1}\,\mathrm{W}^{-1}$; see Supplement 1). Using Eq. (2) we calculate the product of pulse energy and FWHM duration to be 22.7 pJ·ps, which is quite close to the measured value of 14.1 pJ·ps (calculated from Fig. 3). The disparity is most likely due to an underestimation of the intracavity pulse energy in the experiments.

Soliton fiber ring lasers can be stably mode-locked at a high harmonic of the round-trip frequency using optoacoustic interactions at few-gigahertz frequencies in the small glass core of a PCF. Pulse repetition rates of ~2 GHz, durations of ~500 fs, and energies of tens of picojoules are typically achieved with short-term pulse amplitude noise of ~0.1% over a bandwidth of 1 Hz to 1 MHz, and pulse timing jitter ~40 fs over a bandwidth of 100 Hz to 1 MHz.

The authors thank T. Roethlingshoefer and B. Stiller from the Leuchs Division at MPL for providing some components and equipment for the experiments.

See Supplement 1 for supporting content.

REFERENCES

1. M. E. Fermann, A. Galvanauskas, and G. Sucha, *Ultrafast Lasers Technology and Applications* (Dekker, 2003).
2. M. E. Fermann and I. Hartl, Nat. Photonics **7**, 868 (2013).
3. L. E. Nelson, D. J. Jones, K. Tamura, H. A. Haus, and E. P. Ippen, Appl. Phys. B **65**, 277 (1997).
4. M. E. Fermann, Appl. Phys. B **58**, 197 (1994).
5. I. N. Duling III, Opt. Lett. **16**, 539 (1991).
6. K. Tamura, E. P. Ippen, H. A. Haus, and L. E. Nelson, Opt. Lett. **18**, 1080 (1993).
7. Z. Sun, T. Hasan, F. Torrisi, D. Popa, G. Privitera, F. Wang, F. Bonaccorso, D. M. Basko, and A. Ferrari, ACS Nano **4**, 803 (2010).
8. J. J. McFerran, L. Nenadovic, W. C. Swann, J. B. Schlager, and N. R. Newbury, Opt. Express **15**, 13155 (2007).
9. A. Martinez and S. Yamashita, Opt. Express **19**, 6155 (2011).
10. H. Chen, Z. Haider, J. Lim, S. Xu, Z. Yang, F. X. Kaertner, and G. Chang, Opt. Lett. **38**, 4927 (2013).
11. H. Byun, M. Y. Sander, A. Motamedi, H. Shen, G. S. Petrich, L. A. Kolodziejski, E. P. Ippen, and F. X. Kaertner, Appl. Opt. **49**, 5577 (2010).
12. H. Takara, S. Kawanishi, M. Saruwatari, and K. Noguchi, Electron. Lett. **28**, 2095 (1992).
13. T. F. Carruthers, I. N. Duling III, M. Horowitz, and C. R. Menyuk, Opt. Lett. **25**, 153 (2000).
14. M. W. Phillips, A. I. Ferguson, G. S. Kino, and D. B. Patterson, Opt. Lett. **14**, 680 (1989).
15. E. Yoshida, Y. Kimura, and M. Nakazawa, Appl. Phys. Lett. **60**, 932 (1992).
16. M. L. Dennis and I. N. Duling III, Electron. Lett. **28**, 1894 (1992).
17. B. C. Collings, K. Bergman, and W. H. Knox, Opt. Lett. **23**, 123 (1998).
18. K. S. Abedin, J. T. Gopinath, L. A. Jiang, M. E. Grein, H. A. Haus, and E. P. Ippen, Opt. Lett. **27**, 1758 (2002).
19. A. B. Grudinin and S. Gray, J. Opt. Soc. Am. B **14**, 144 (1997).
20. A. N. Pilipetskii, E. A. Golovchenko, and C. R. Menyuk, Opt. Lett. **20**, 907 (1995).
21. P. Dainese, P. St. J. Russell, G. S. Wiederhecker, N. Joly, H. L. Fragnito, V. Laude, and A. Khelif, Opt. Express **14**, 4141 (2006).
22. M. S. Kang, A. Nazarkin, A. Brenn, and P. St. J. Russell, Nat. Phys. **5**, 276 (2009).
23. M. S. Kang, A. Brenn, and P. St.J. Russell, Phys. Rev. Lett. **105**, 153901 (2010).
24. L. Xiao, M. S. Demokan, W. Jin, Y. Wang, and C. L. Zhao, J. Lightwave Technol. **25**, 3563 (2007).
25. M. S. Kang, N. Y. Joly, and P. St. J. Russell, Opt. Lett. **38**, 561 (2013).
26. M. Pang, X. Jiang, G. K. L. Wong, G. Onishchukov, N. Y. Joly, G. Ahmed, and P. St. J. Russell, *Advanced Photonic 2014* (Optical Society of America, 2014), paper NTh4A.5.
27. B. Stiller and T. Sylvestre, Opt. Lett. **38**, 1570 (2013).
28. M. Hofer, M. E. Fermann, F. Haberl, M. H. Ober, and A. J. Schmidt, Opt. Lett. **16**, 502 (1991).
29. M. Salhi, H. Leblond, and F. Sanchez, Phys. Rev. A **67**, 013802 (2003).
30. S. M. J. Kelly, Electron. Lett. **28**, 806 (1992).
31. D. von der Linde, Appl. Phys. B **39**, 201 (1986).
32. H. A. Haus and A. Mecozzi, IEEE J. Quantum Electron. **29**, 983 (1993).
33. G. P. Agrawal, *Nonlinear Fiber Optics* (Academic, 2007).
34. R. W. Boyd, *Nonlinear Optics* (Academic, 2008).
35. M. Nakazawa, E. Yoshida, and K. Tamura, Electron. Lett. **32**, 1285 (1996).
36. K. K. Gupta, D. Novak, and H. Liu, IEEE J. Quantum Electron. **36**, 70 (2000).

optica

Stable subpicosecond soliton fiber laser passively mode-locked by gigahertz acoustic resonance in photonic crystal fiber core: supplementary materials

M. PANG,[1,*] X. JIANG,[1] W. HE,[1] G. K. L. WONG,[1] G. ONISHCHUKOV,[1] N. Y. JOLY,[1] G. AHMED,[1] C. R. MENYUK,[2] AND P. ST.J. RUSSELL[1]

[1]*Max Planck Institute for the Science of Light, Guenther-Scharowsky-Strasse 1, 91058 Erlangen, Germany*
[2]*Department of Computer Science and Electrical Engineering, University of Maryland Baltimore County, Baltimore, MD, 21250, USA*
**Corresponding author: meng.pang@mpl.mpg.de*

Published 30 March 2015

This document provides supplementary information to "Stable subpicosecond soliton fiber laser passively mode-locked by gigahertz acoustic resonance in photonic crystal fiber core," http://dx.doi.org/10.1364/optica.2.000339. We provide a detailed description of the acoustic wave generation in the solid-core silica photonic crystal fiber and some additional system parameters and experimental results.

http://dx.doi.org/10.1364/optica.2.000339.s001

1. Acoustic wave generation

We begin with the acoustic wave equation driven by an electrostrictive effect [S1]:

$$\frac{\partial^2 \rho}{\partial t^2} - v_a^2 \left(1 + \Gamma \frac{\partial}{\partial t}\right) \nabla^2 \rho = \nabla \cdot \boldsymbol{f} \qquad \textbf{(S1)}$$

where ρ is the material density variation from its mean value of ρ_0, v_a is the sound velocity, Γ is the damping factor of the acoustic wave and $\boldsymbol{f}$ is the driving stress created through electrostriction [S1]:

$$\boldsymbol{f} = -\frac{1}{2} \varepsilon_0 \gamma_e \nabla \overline{E^2} \qquad \textbf{(S2)}$$

where ε_0 is the electric permittivity in vacuum, γ_e is the electrostrictive constant of fused silica, and E is the electric field of the linearly polarized light propagating in the PCF.

The driving optical pulse train has repetition rate Ω and individual pulse energies of E_P. The fundamental optical mode in the PCF has the largest overlap integral with the first-order radial (R_{01}) acoustic mode [S2], and in practice the repetition rate of the pulsed light is close to the resonance frequency of this acoustic mode, while the resonance linewidth is quite narrow (mechanical quality factor ~250 [S2]). If we consider only the fundamental frequency component of the optical pulse train and neglect optical loss (<0.05 dB/m) in the PCF, the electrostrictive term driving the R_{01} acoustic mode is given by [S2]:

$$\nabla \cdot \boldsymbol{f} = -\frac{1}{4} \varepsilon_0 \gamma_e s_1 \nabla_\perp^2 E_0^2 e^{i(\Omega t - qz)} + \text{c.c.} \qquad \textbf{(S3)}$$

where E_0 is the normalized field distribution of the optical mode in the PCF core, q its propagation constant, $\nabla_\perp^2$ the transverse Laplacian operator, and s_1 is given by:

$$s_1 \approx \frac{1}{T_P} \int_{-T_P/2}^{T_P/2} A^2(z,t)\, dt = \frac{E_p \Omega}{\pi n_{\text{eff}} \varepsilon_0 c A_{\text{eff}}} \qquad \textbf{(S4)}$$

where $A(z,t)$ is the slowly varying pulse envelope, $T_P = 2\pi/\Omega$ is time between pulses, n_{eff} the effective refractive index, A_{eff} the effective mode area of the optical mode and c is the speed of light in vacuum. In Eq. (S4) the duration of the optical pulse is assumed to be much shorter than the period of the excited acoustic wave.

The acoustic modes supported by the PCF core are given by the modal equation [S3] as:

$$\nabla_\perp^2 \rho_{mn}(r,\theta) + \left(\frac{\Omega_{mn}^2}{v_a^2} - q^2\right) \rho_{mn}(r,\theta) = 0 \qquad \textbf{(S5)}$$

where $\rho_{mn}(r,\theta)$ is the normalized mode profile of different acoustic modes and Ω_{mn} is the eigenfrequency of the (m, n)-th acoustic mode. Using finite element modelling and setting q equal to zero, we can simulate the density variation distribution of acoustic modes supported by the PCF structure (scanning electron micrograph of the PCF is shown in Fig. 1). The simulations predict

that the R_{01} acoustic mode has a resonant frequency Ω_{01} = 2.05 GHz, which is reasonably close to the measured value of 2.13 GHz [S2]. Its acoustic mode profile is shown in Fig. S1a, the fundamental optical mode profile in silica being shown in Fig. S1b for comparison. We also numerically calculated the magnitude of the overlap integral between the fundamental optical mode and the R_{01} acoustic mode to be 2.4 μm^{-2}.

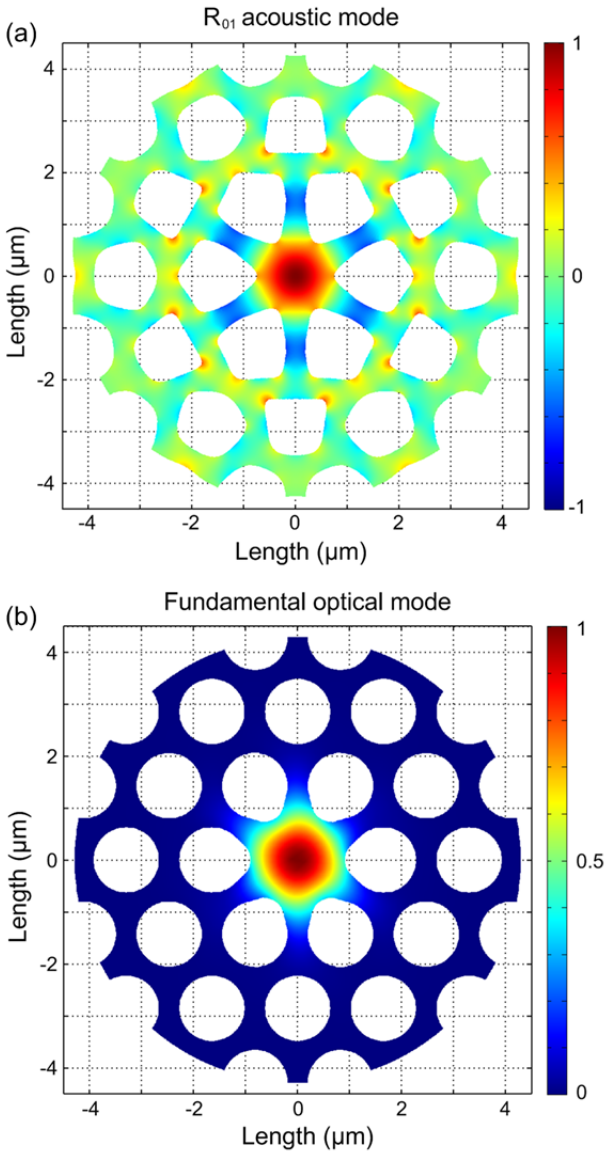

Fig. S1. (a) Simulated normalized density variation (color map) and material deformation of the R_{01} acoustic mode in the PCF profile. (b) Normalized electric field distribution (color map) of the fundamental optical mode in the silica PCF.

By inserting Eq. (S3), Eq. (S4) and Eq. (S5) into Eq. (S1), we obtain the steady-state equation as:

$$-ib\rho_{01}(r,\theta)\Omega\Gamma_B - b\rho_{01}(r,\theta)(\Omega^2-\Omega_{01}^2) = -\frac{1}{2}\varepsilon_0\gamma_e\nabla_\perp^2 E_0^2\cdot s_1 \quad \textbf{(S6)}$$

where b is the amplitude, $\rho_{01}(r,\theta)$ is the normalized mode profile, and $\Gamma_B = \Omega_{01}^2\Gamma$ is the Brillouin linewidth of the R_{01} acoustic mode. Finally by multiplying both sides of Eq. (S6) by $\rho_{01}(r,\theta)$ and integrating over the transverse plane, we obtain:

$$b = \frac{-\varepsilon_0\gamma_e s_{01}\left\langle\rho_{01}(r,\theta)\nabla_\perp^2 E_0^2\right\rangle}{2(\Omega_{01}^2-\Omega^2-i\Omega\Gamma_B)\left\langle\rho_{01}^2(r,\theta)\right\rangle} \quad \textbf{(S7)}$$

where we denote integrated quantities by angle brackets as $\langle f(r)\rangle = \int_0^{2\pi}\int_0^{+\infty} f(r,\theta)rdrd\theta$, and $Q = \left\langle\rho_{01}(r,\theta)\nabla_\perp^2 E_0^2\right\rangle / \left\langle\rho_{01}^2(r,\theta)\right\rangle$ is the overlap integral of the R_{01} acoustic mode with the electrostrictive stress field. Thus the acoustic wave generated by the driving optical pulses may be written as:

$$\rho(z,t,r,\theta) = \frac{\gamma_e |Q| E_p\rho_{01}(r,\theta)e^{i(\Omega t-qz)}}{4\pi n_{eff}cA_{eff}[2(\Omega_{01}-\Omega)-i\Gamma_B]} + \text{c.c.} \quad \textbf{(S8)}$$

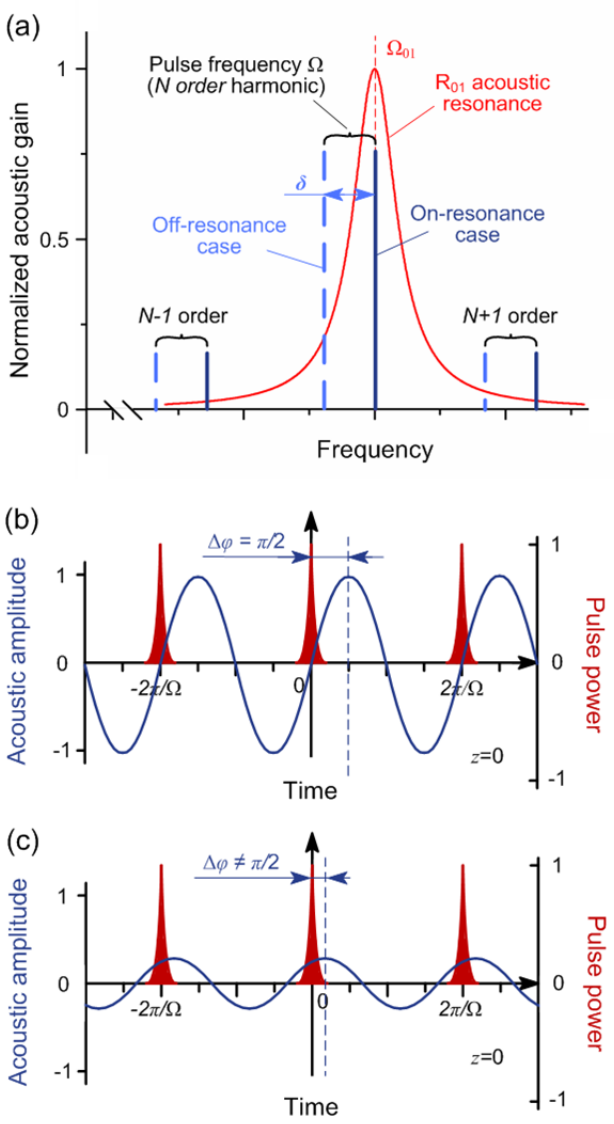

Fig. S2. (a) Gain spectrum of an acoustic mode with resonant frequency Ω_{01}. Repetition rate of the driving pulse train is at the N^{th} order harmonic of the cavity round-trip frequency. Full blue line: on-resonance case $\Omega = \Omega_{01}$. Light-blue dashed line: off-resonance case $\Omega \neq \Omega_{01}$. (b) The $\pi/2$ relative phase shift between the acoustic wave and its driving pulse train in the on-resonance case. (c) Illustrating the decrease in acoustic amplitude, and shift in acoustic phase, when the repetition rate of the driving pulse train is detuned from the acoustic resonant frequency.

In the experiments, the repetition rate Ω of the optical pulses is equal to an integer multiple of the round-trip frequency (N^{th} order harmonic as shown in Fig. S2a), while the resonant frequency Ω_{01}

of the R_{01} acoustic mode is given by the PCF structure. We denote the frequency difference between them as $\delta = \Omega - \Omega_{01}$, and by using Eq. (S8) the acoustic wave can be expressed as:

$$\rho(z,t,r,\theta) = \frac{\gamma_e |Q| E_p \rho_{01}(r,\theta) e^{i(\Omega t - qz - \Delta\varphi)}}{4\pi n_{eff} c A_{eff} \sqrt{4\delta^2 + (\Gamma_B)^2}} + \text{c.c.} \quad \textbf{(S9)}$$

where $\Delta\varphi$ is the relative phase offset between the acoustic wave and its driving pulse train given by:

$$\Delta\varphi = \text{arccot}(-2\delta / \Gamma_B), \quad 0 \le \Delta\varphi \le \pi \quad \textbf{(S10)}$$

From Eq. (S9), we see that the amplitude of the generated acoustic wave is inversely proportional to $(4\delta^2 + \Gamma_B^2)^{1/2}$. Acoustic gain appears when the phase shift $\Delta\varphi$ between the driving pulse train and the acoustic wave (Eq. (S10)) lies within the range of (0, π) [S1,S2]. In a manner similar to a driven oscillator with a single degree of freedom [S4], the amplitude of the acoustic wave reaches its maximum value in the on-resonance case ($\delta = 0$) as illustrated in Fig. S2b, where $\Delta\varphi = \pi/2$. In the off-resonance case $\Delta\varphi \neq \pi/2$ (Fig. S2c) and the amplitude of the acoustic wave decreases.

Using Eq. (S8) we can obtain the modulation of material relative permittivity $\Delta\varepsilon_r(z,t,r,\theta)$ due to the optoacoustic effect:

$$\Delta\varepsilon_r(z,t,r,\theta) = \gamma_e \frac{\rho}{\rho_0} = \frac{\gamma_e^2 |Q| E_p \rho_{01}(r,\theta) e^{i(\Omega t - qz - \Delta\varphi)}}{4\pi n_{eff} c A_{eff} \rho_0 \sqrt{4\delta^2 + (\Gamma_B)^2}} + \text{c.c.} \quad \textbf{(S11)}$$

Using Eq. (S10) and Eq. (S11) we can roughly estimate the amplitude of the index modulation generated by the optical pulses in the center of the PCF core. When the PCF has a core diameter of 1.8 μm corresponding to an effective mode area of 2.54 μm^2 and the pulse energy is 25 pJ, by using γ_e = 1.17, $|Q|$ = 2.4 μm^{-2}, n_{eff} = 1.46, c = 3×10^8 m/s, ρ_0 = 2.2 ×10^3 kg/m^3, $\delta = 2\pi\times5$ MHz and $\Gamma_B = 2\pi\times8.1$ MHz, we obtain that $\Delta\varphi = 0.22\pi$ with a generated refractive index modulation of ~2×10^{-8}, which is around two orders of magnitude larger than the optoacoustic-induced index modulation in conventional step-index fiber [S5,S6].

2. Kerr nonlinearity and dispersion maps in the laser cavity

The 0.6 m length of PCF has Kerr nonlinearity 36.3 km^{-1}W^{-1} and dispersion –119 ps^2/km at 1560 nm. The 0.2 m length of highly nonlinear fiber (HNLF) has Kerr nonlinearity 10.3 km^{-1}W^{-1} and dispersion 19.8 ps^2/km, and the 0.6 m erbium-doped fiber a Kerr nonlinearity of 9.3 km^{-1}W^{-1} and a dispersion of 77 ps^2/km. The remaining fiber in the cavity is conventional SMF28 with length of 10.8 m, a Kerr nonlinearity of 1.1 km^{-1}W^{-1} and a dispersion of –22.8 ps^2/km. We calculated a cavity-average Kerr nonlinearity coefficient of 3.4 km^{-1}W^{-1} and a group-velocity dispersion of –21.9 ps^2/km. Then, based on the fundamental soliton assumption [S7], the product of pulse energy and FWHM duration would be 22.7 pJ·ps, which is quite close to the value of 14.1 pJ·ps estimated from the experimental results.

The Kerr nonlinearity dominates the pulse shape (leading to soliton formation in the steady state), whereas the much slower optoacoustic nonlinearity locks the pulse repetition rate. While the fast saturable absorber (based on nonlinear polarization rotation) does not really contribute to pulse shaping, it plays an important role in helping the laser self-start as well as stabilizing the mode-locking by suppressing the background radiation.

3. Amplitude noise and timing jitter

To estimate the short-term pulse amplitude noise, the laser baseband single-sideband (SSB) noise spectrum was measured as a function of off-set frequency from 0 Hz. The results are shown in Fig. S3a, with the noise floor of the 26 GHz electrical spectrum analyzer (ESA) and 30 GHz photodetector as a reference. In this baseband noise spectrum, sharp peaks at ~1 kHz correspond to acoustic/vibrational perturbations. By integrating this baseband noise, we estimate the relative amplitude noise to be ~0.1% over a bandwidth from 1 Hz to 1 MHz [S8,S9].

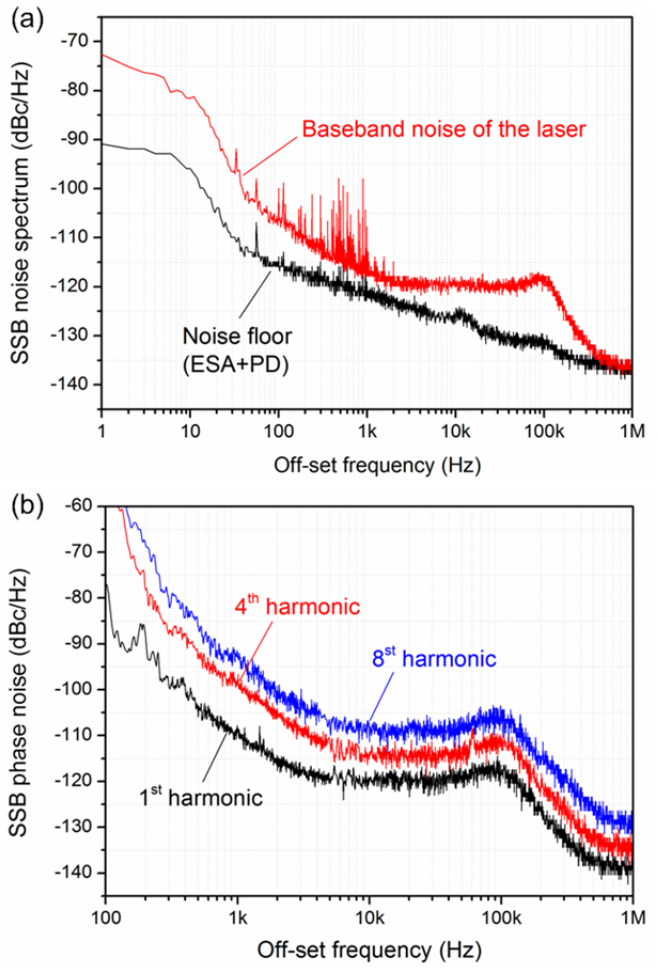

Fig. S3. (a) Measured baseband SSB noise spectrum of the laser (red curve), and noise floor of the ESA and photodetector (black curve). (b) Measured SSB phase noise spectra for 1st, 4th and 8th harmonics of the pulse repetition frequency.

We also estimated the pulse timing jitter by measuring the SSB noise spectra for different harmonics of the pulse repetition rate. The spectra of the 1st, 4th and 8th harmonics, measured over a frequency range from 100 Hz to 1 MHz, are shown in Fig. S3b. It can be clearly seen that the noise increases strongly for higher harmonic orders, giving direct evidence of temporal jitter in the pulse train [S8]. In this free-running laser without cavity length stabilization, phase noise at low frequencies (<10 kHz) is dominated by cavity length perturbations, thus the low-frequency pulse timing jitter should be similar to that of a typical free-running laser mode-locked at the cavity round-trip frequency. Gordon-Haus jitter may be the main noise source at high frequencies. Strong phase modulation through enhanced optoacoustic interactions in the PCF may re-time the pulses and suppress high-frequency timing jitter, just as in lasers that are actively mode-locked with an external phase modulator [S10].

We estimate the relative pulse timing jitter using the expression $\Delta T/T = (2P_{noise})^{1/2}/(2\pi)$ [S9,S10], where T is the time between pulses, ΔT is the timing jitter and P_{noise} is the SSB noise power integrated over the selected frequency range. The value is ~40 fs from 100 Hz to 1 MHz and ~26 fs from 10 kHz to 1 MHz. Since the accuracy of these noise measurements using an ESA is limited by the intrinsic amplitude and phase noise of the ESA and the photodetector [S11], the estimated values give only upper limits for the laser amplitude noise and pulse timing jitter.

The pulse energy fluctuations and timing jitter at the fundamental cavity round-trip frequency (i.e., the super-mode noise of the harmonically mode-locked laser [S12]) are at low levels, with a super-mode suppression ratio >50 dB. In the experiment, we observed super-mode noise peaks with small amplitudes and narrow linewidths, off-set from the main comb-lines by multiples of the cavity round-trip frequency f_{RT}. Those super-mode peaks are due to correlated high-frequency noise in the pulse envelope [S10,S12].

4. Optical comb structure

We also measured the optical comb structure by heterodyning with a local oscillator signal from a fiber laser with 2 kHz linewidth at 1550 nm. A tunable optical filter (~12 nm bandwidth) was inserted into the cavity and used to tune the central wavelength of the laser close to that of the local oscillator. This filter increased the overall cavity length, reducing the mode-spacing from 16.8 to 13.1 MHz but otherwise having no effect on the lasing characteristics. The beat signal between the mode-locked laser and the local oscillator was measured using a photodetector and the ESA, and the results are shown in Fig. S4. Similar to the case of active high-harmonic mode-locking with a phase modulator [S10,S13], the optical comb structure shows cavity modes with 13.1 MHz spacing (note that frequencies above and below the local oscillator frequency cannot be distinguished in this measurement, resulting in two interleaved frequency combs). We believe that the sub-peaks offset by ~1 MHz from the comb lines are artefacts of the local oscillator. The amplitude fluctuations among different comb lines are mainly induced by wavelength drift in both lasers, which shifts the line positions within the measurement time. Decreasing the sweep time of the ESA by using a narrower span and lower resolution can significantly decrease the amplitude fluctuations, however, this would mean that the comb structure could not be so well resolved. As shown in Fig. S4b, the linewidth of an individual comb line is less than 20 kHz (the resolution limit of the ESA).

When the system is stably mode-locked, each soliton circulating in the laser cavity must restore itself (both in phase and in amplitude) after each cavity round-trip, which yields narrow linewidths for the optical comb lines. Preliminary measurements of the heterodyne signal using a fast oscilloscope show that although individual solitons within one cavity round-trip time have arbitrary relative phases, this phase relationship repeats periodically after every round-trip. This is similar to what happens in conventional active mode-locking using a phase modulator [S10,S13].

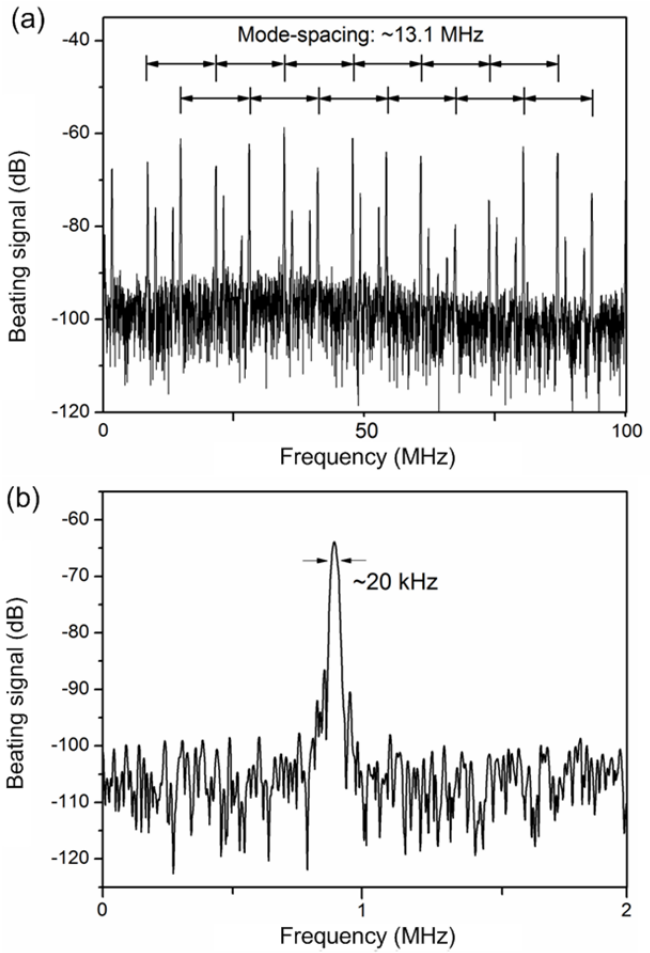

Fig. S4. (a) Heterodyne signal measured by the ESA with 100 kHz resolution bandwidth and (b) a single comb line measured with 20 kHz resolution.

References

S1. R. W. Boyd, Nonlinear Optics (Academic Press, 2008).
S2. M. S. Kang, A. Nazarkin, A. Brenn and P. St.J. Russell, Nat. Phys. **5**, 276 (2009).
S3. A. Kobyakov, M. Sauer, and D. Chowdbury, Advance in Opt. and Photon. **2**, 1 (2004).
S4. B. H. Tongue, Principles of Vibration (Oxford University Press, 2002).
S5. A. B. Grudinin and S. Gray, J. Opt. Soc. Am. B **14**, 144 (1997).
S6. J. K. Jang, M. Erkintalo, S. G. Murdoch, and S. Coen, Nat. Photon. **7**, 657 (2013).
S7. G. P. Agrawal, Nonlinear Fiber Optics (Academic Press, 2007).
S8. D. von der Linde , Appl. Phys. B. **39**, 201 (1986).
S9. H. A. Haus and A. Mecozzi, J. Quantum Electron. **29**, 983 (1993).
S10. M. E. Grein, A. Haus, Y. Chen and E. P . Ippen, J. Quantum Electron. **40**, 1458 (2004).
S11. J. Kim, J. Chen, J. Cox and F. Kartner, Opt. Lett. **32**, 3519 (2007).
S12. F. Rana, H. L. T. Lee, R. J. Ram, M. E. Grein, L. A. Jiang, E. P. Ippen and H. A. Haus, J. Opt. Soc. Am. B. **19**, 2609 (2002).
S13. M. E. Grein, L. A. Jiang, H. A. Haus and E. P. Ippen, Opt. Lett. **27**, 957 (2002).